Powell–Sabin Spline Wavelets

Evelyne Vanraes
Jan Maes
Adhemar Bultheel

Report TW 362, July 2003



Katholieke Universiteit Leuven
Department of Computer Science
Celestijnenlaan 200A – B-3001 Heverlee (Belgium)

Powell–Sabin Spline Wavelets

Evelyne Vanraes
Jan Maes
Adhemar Bultheel

Report TW 362, July 2003

Department of Computer Science, K.U.Leuven

Abstract

Recently we developed a subdivision scheme for Powell–Sabin splines. It is a triadic scheme and it is general in the sense that it is not restricted to uniform triangles, the vertices must not have valence six and there are no restrictions on the initial triangulation. A sequence of nested spaces or multiresolution analysis can be associated with the base triangulation. In this paper we use the lifting scheme to construct basis functions for the complement space that captures the details that are lost when going to a coarser resolution. The subdivision scheme appears as the first lifting step or prediction step. A second lifting step, the update, is used to achieve certain properties for the complement spaces and the wavelet functions such as orthogonality and vanishing moments. The design of the update step is based on stability considerations. We prove stability for both the scaling functions and the wavelet functions.

Keywords : Powell–Sabin splines, subdivision, multiresolution, wavelets, lifting, stability.
AMS(MOS) Classification : 65D07, 65D17, 68U07.

Powell–Sabin Spline Wavelets

Evelyne Vanraes, Jan Maes, Adhemar Bultheel

July 2003

Abstract

Recently we developed a subdivision scheme for Powell–Sabin splines. It is a triadic scheme and it is general in the sense that it is not restricted to uniform triangles, the vertices must not have valence six and there are no restrictions on the initial triangulation. A sequence of nested spaces or multiresolution analysis can be associated with the base triangulation. In this paper we use the lifting scheme to construct basis functions for the complement space that captures the details that are lost when going to a coarser resolution. The subdivision scheme appears as the first lifting step or prediction step. A second lifting step, the update, is used to achieve certain properties for the complement spaces and the wavelet functions such as orthogonality and vanishing moments. The design of the update step is based on stability considerations. We prove stability for both the scaling functions and the wavelet functions.

Keywords: Powell–Sabin splines, subdivision, multiresolution, wavelets, lifting, stability.

AMS(MOS) classification: 65D07, 65D17, 68U07.

1 Introduction

Powell–Sabin splines are functions in the space $S_2^1(\Delta_{PS})$ of C^1 continuous piecewise quadratic functions on a Powell–Sabin refinement. Such a refinement Δ_{PS} can be obtained from an arbitrary triangulation Δ by splitting each triangle into six subtriangles with a common interior point [9]. Working with triangles makes it possible to design surfaces with an arbitrary number of edges, which is not possible with the often used tensor product B–spline representation that is restricted to rectangular domains. In contrast to Bézier triangles [5], where imposing smoothness conditions between the patches requires a great number of nontrivial relations between the coefficients to be satisfied, the C^1 continuity of a PS–spline is guaranteed for any choice of the coefficients.

A first attempt to describe PS–splines was by Shi *et al.* [11], but their construction method had some serious drawbacks from the numerical point of view. This was solved by the improved algorithm of Dierckx [4] to construct a B–spline basis. This representation has the advantage that the basis functions form a convex partition of unity which is a useful property in CAGD applications. Furthermore it leads to a nice geometric interpretation with control triangles that are tangent to the surface. The last advance in the area of Powell–Sabin splines is the development of a subdivision scheme [17]. Given a surface on a certain triangulation, we can now calculate a B–spline representation of the surface on a refinement of that triangulation. The result is a denser set of control points.

Lounsbery *et al.* [6] show that with every subdivision scheme, a sequence of nested spaces with corresponding basis functions, the scaling functions, can be associated. It is then possible to construct wavelets, that is, a set of functions that span the sequence of orthogonal complement spaces by imposing a least–squares condition when restricting the approximation to the scaling functions. Locally supported wavelets are obtained by relaxing the condition that the wavelets should lie in the

orthogonal complement spaces. This is immediately related to the technique of the lifting scheme [13, 3] in which locally supported biorthogonal wavelets are build using consecutive lifting steps.

In this paper we use lifting to construct Powell–Sabin spline wavelets. The same idea is used by Windmolders *et al.* for the uniform case [18]. The subdivision scheme appears in the lifting algorithm as the prediction step. Without any further lifting steps the wavelets are the scaling functions corresponding to the in between vertices on the finer level. These wavelets are far from orthogonal to the scaling functions and possess no vanishing moments. However, from stability analysis [2, 12, 16] we know that these are important properties. Therefor we add a second lifting step that projects the wavelets in the desired complement space.

Section 2 gives a short overview of Powell–Sabin splines and introduces a normalisation of the basis functions with respect to their support because of stability. Section 3 recalls the subdivision algorithm and associates a sequence of nested subspaces with the base triangulation. In section 4 we study the complement space and describe the filter bank algorithm in terms of lifting steps. Then in section 5 we discuss the design of the update step in detail. Finally, section 6 gives the results and a proof of stability of the wavelet transform.

2 Powell–Sabin splines

We are interested in signals representing splines in $S_1^2(\Delta_{PS})$, that is the space of C^1 continuous quadratic functions on a Powell–Sabin refinement Δ_{PS}. In this section we recall the B–spline representation and the geometric interpretation with control triangles. Then we introduce a normalisation of the basis functions with respect to their support so that they form a $\mathbf{L}_p$–stable basis.

2.1 B–spline representation for the space $S_1^2(\Delta_{PS})$

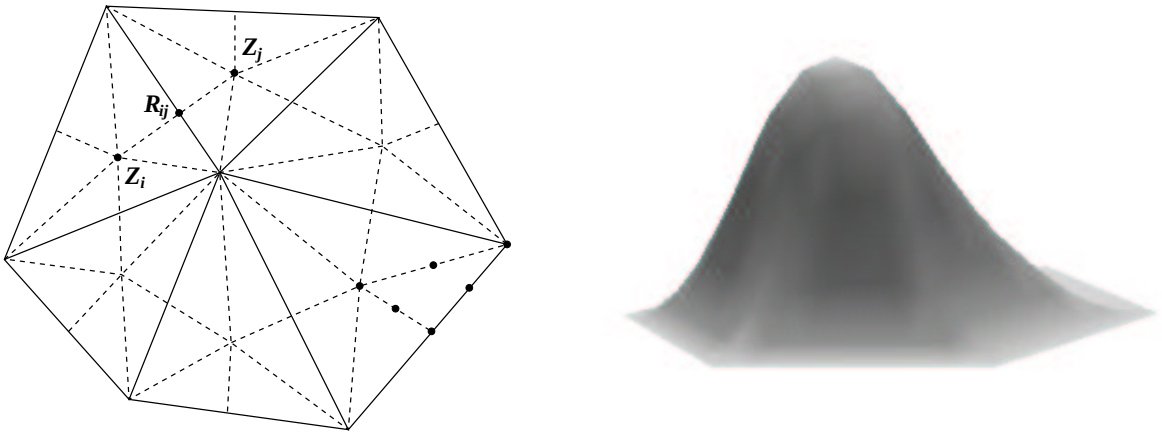
Consider a simply connected subset $\Omega \subset \mathbb{R}^2$ with polygonal boundary $\delta\Omega$. Suppose we have a conforming triangulation Δ of Ω, constituted of triangles ρ_j, $j = 1, \ldots, t$, vertices V_k with Cartesian coordinates (x_k, y_k), $k = 1, \ldots, n$. Then Δ_{PS} is a Powell–Sabin refinement of Δ, which divides each triangle ρ_j into six smaller triangles with a common vertex Z_j as follows (figure 1a) :

(1) Choose an interior point Z_j in each triangle ρ_j, so that if two triangles ρ_i and ρ_j have a common edge, then the line joining these interior points Z_i and Z_j intersects the common edge at a point R_{ij} between its vertices.
(2) Join each point Z_j to the vertices of ρ_j.
(3) For each edge of the triangle ρ_j
   - which belongs to the boundary $\delta\Omega$, join Z_j to an arbitrary point of the edge.
   - which is common to a triangle ρ_i, join Z_j to R_{ij}.

Now we consider the space of piecewise C^1 continuous quadratic polynomials on Δ_{PS}, the Powell–Sabin splines. Each of the $6t$ triangles resulting from the PS–refinement becomes the domain triangle of a quadratic bivariate Bézier polynomial [5]. Powell and Sabin [9] proved that the dimension of $S_2^1(\Delta_{PS})$ equals $3n$: there exists a unique solution $s(x, y) \in S_2^1(\Delta_{PS})$ for the interpolation problem

$$s(V_k) = f_k, \quad \frac{\partial s}{\partial x}(V_k) = f_{x,k}, \quad \frac{\partial s}{\partial y}(V_k) = f_{y,k}, \quad k = 1, \ldots, n. \tag{2.1}$$

So given the function and derivative values at each vertex V_k of Δ, the spline is uniquely defined.



(a) (b)

Figure 1. (a) PS–refinement. Each triangle ρ_j is split into six smaller triangles with a common vertex Z_j. (b) B–spline basis function.

Dierckx [4] showed that each piecewise polynomial $s(x,y) \in S_2^1(\Delta_{PS})$ has a unique representation

$$s(x,y) = \sum_{i=1}^{n} \sum_{j=1}^{3} c_{ij} B_{ij}(x,y) \ , \quad (x,y) \in \Omega, \tag{2.2}$$

where the basis functions form a convex partition of unity

$$B_{ij}(x,y) \geq 0, \tag{2.3}$$

$$\sum_{i=1}^{n} \sum_{j=1}^{3} B_{ij}(x,y) \equiv 1, \tag{2.4}$$

and have local support: $B_{ij}(x,y)$ is nonzero only on the so–called molecule M_i of V_i, being the set of triangles ρ_l that have V_i as a vertex. One such basis function is depicted in figure 1b. Note that three basis functions are associated with each vertex in Δ.

We will find it convenient to write equation (2.2) in matrix form as

$$s(x,y) = \mathbf{B}\ \mathbf{c}, \tag{2.5}$$

where $\mathbf{B}$ denotes the row vector of basis functions $B_{ij}(x,y)$ and $\mathbf{c}$ the column vector with the coefficients c_{ij} in the expansion.

2.2 Geometric interpretation

For each vertex V_i there is a PS–triangle $t_i(Q_{i1}, Q_{i2}, Q_{i3})$ that determines the three basis functions. This triangle must contain a specific set of Bézier domain points that are called the PS–points. We define the control points as

$$C_{ij} = (Q_{ij}, c_{ij}) = (X_{ij}, Y_{ij}, c_{ij}). \tag{2.6}$$

The three control points of a vertex V_i together form a triangle that is called the control triangle T_i

$$T_i(C_{i1}, C_{i2}, C_{i3}). \tag{2.7}$$

The projection of the control triangles T_i in the (x, y) plane are the PS–triangles t_i. One can prove that the control triangle T_i is tangent to the surface $z = s(x, y)$ at V_i. For design purposes we prefer the control points of the corresponding control triangle to be close to the surface. In [4] the PS–triangle with the smallest area is computed, but other choices are possible [15].

2.3 Stability of the B–spline basis

The set $\mathbf{B} := \{B_{ij}(x, y)\}$ is a Riesz basis if

$$m\|\mathbf{c}\| \leq \|\mathbf{B}\ \mathbf{c}\| \leq M\|\mathbf{c}\| \tag{2.8}$$

for all choices of the coefficient vector $\mathbf{c}$ and with $0 < m, M < \infty$ depending only on the smallest angle θ_Δ in the triangulation Δ. The constants m and M are called the lower and upper Riesz bounds, and the ratio M/m is the condition number $\kappa(\mathbf{B})$ of the basis.

Maes *et al.* [7] give explicit expressions for the Riesz bounds for the ∞-norm in case the interior points Z in the PS–refinement are chosen as the incenters of the triangles. Similar expressions for other common choices such as the barycenter can easily be found.

Theorem 2.1 $\mathbf{B}$ *forms a* $\mathbf{L}_\infty$*–stable basis in the sense that there exists a constant* K_1 *dependent only on* θ_Δ *such that*

$$\frac{1}{K_1}\|\mathbf{c}\|_\infty \leq \|\mathbf{B}\ \mathbf{c}\|_\infty \leq \|\mathbf{c}\|_\infty \tag{2.9}$$

for all choices of the coefficient vector $\mathbf{c}$.

Proof. see [7]

For the construction of the wavelets we use an inner product to define orthogonal spaces. Consequently we are interested in the 2-norm induced by the inner product. To have a $\mathbf{L}_p$-stable basis the basis functions in $\mathbf{B}$ need to be normalised with respect to their support. The result is established in theorem 2.4, but first we give two lemmas on triangles and triangulations that are needed for the proof.

Lemma 2.2 *Consider a triangle* ρ. *Define* R_ρ *as the diameter of the smallest disk containing* ρ, r_ρ *as the radius of the largest disk contained in* ρ *and* θ_ρ *as the smallest angle in* ρ. *Then*

$$\frac{R_\rho}{r_\rho} \leq \frac{4}{\tan(\theta_\rho/2)}. \tag{2.10}$$

Proof. see [7]

Lemma 2.3 *Consider two arbitrary triangles* ρ *and* $\tilde{\rho}$ *in the same molecule* $M_i \in \Delta$. *The fraction of their areas is bounded*

$$\frac{A_{\tilde{\rho}}}{A_\rho} \leq K_2, \tag{2.11}$$

where $K_2 := \left(\frac{1}{\sin(\theta_\Delta)}\right)^{\frac{2\pi}{\theta_\Delta}+2} \frac{16}{\tan(\theta_\Delta/2)^2}$.

Proof. Define $e_{\max}(\rho)$ and $e_{\min}(\rho)$ as the maximum resp. minimum edge of a triangle ρ. The ratio of the areas of the triangles satisfies

$$\frac{A_{\tilde{\rho}}}{A_\rho} \leq \frac{\pi|e_{\max}(\tilde{\rho})|^2}{\pi r_\rho^2}. \tag{2.12}$$

Let e and $\hat{e}$ be two edges of the same triangle ρ, then

$$\sin(\theta_\Delta)|e| \leq |\hat{e}|. \tag{2.13}$$

The maximum number of triangles in a molecule M_i is $2\pi/\theta_\Delta$. Therefor there always exists a sequence of edges of maximum length $\frac{\pi}{\theta_\Delta}+1$ between two edges $e_{\max}(\rho)$ and $e_{\max}(\tilde{\rho})$ in the same molecule M_i:

$$|e_{\max}(\tilde{\rho})| \leq \left(\frac{1}{\sin(\theta_\Delta)}\right)^{\frac{\pi}{\theta_\Delta}+1} |e_{\max}(\rho)|. \tag{2.14}$$

Applying Lemma 2.2 yields

$$\frac{|e_{\max}(\rho)|}{r_\rho} \leq \frac{R_\rho}{r_\rho} \leq \frac{4}{\tan(\theta_\Delta/2)}. \tag{2.15}$$

Combining (2.12), (2.14) and (2.15) completes the proof. □

We now introduce the normalised basis functions $\mathbf{\Phi}$ as

$$\mathbf{\Phi} := \{\phi_l := A_l^{-1/p} B_{ij}(x,y),\ l = 3(i-1)+j\} \tag{2.16}$$

and the normalised coefficients $\mathbf{s}$

$$\mathbf{s} := \{s_l := A_l^{1/p} c_{ij},\ l = 3(i-1)+j\} \tag{2.17}$$

or in matrix form

$$\begin{aligned} \mathbf{\Phi} &:= \mathbf{B}\ \mathbf{D}^{-1}, \\ \mathbf{s} &:= \mathbf{D}\ \mathbf{c}, \end{aligned} \tag{2.18}$$

where $\mathbf{D}$ is a diagonal matrix with as elements the pth root of the areas A_l of the support of the corresponding basis function. The representation (2.5) becomes

$$s(x,y) = \mathbf{B}\ \mathbf{c} = \mathbf{\Phi}\ \mathbf{s}. \tag{2.19}$$

We refer to the ϕ_l and the s_l as scaling functions and scaling coefficients, which is standard terminology.

Theorem 2.4 *$\mathbf{\Phi}$ forms a p–stable basis in the sense that there exist constants k_1 and k_2 dependent only on θ_Δ such that*

$$k_1\|\mathbf{s}\|_p \leq \|\mathbf{\Phi}\ \mathbf{s}\|_p \leq k_2\|\mathbf{s}\|_p \tag{2.20}$$

for all choices of the coefficient vector $\mathbf{s}$ and $1 \leq p \leq \infty$.

Proof. We only treat the case $1 \leq p < \infty$. For $p = \infty$ the normalisation factor equals one and we find theorem 2.1. Write $s = \sum_l s_l \phi_l$. Choose a triangle $\rho \in \Delta$, and let $I_\rho := \{l : \mathrm{supp}(\phi_l) \cap \rho \neq 0\}$. Let $1/p + 1/q = 1$, then by Hölder's inequality

$$\int_\rho |s(x,y)|^p = \int_\rho |\sum_{l\in I_\rho} s_l\ A_l^{-1/p} B_{ij}|\ , \quad l = 3(i-1)+j \tag{2.21}$$

$$\leq \sum_{l\in I_\rho} |s_l|^p \int_\rho \left(\sum_{l\in I_\rho} A_l^{-q/p} (B_{ij})^q\right)^{\frac{p}{q}}. \tag{2.22}$$

Since $\#I_\rho \leq 9$ and ϕ_l is uniform bounded

$$\int_\rho |s(x,y)|^p \leq 9^{p/q} \max_{l \in I_\rho} \frac{A_\rho}{A_l} \sum_{l \in I_\rho} |s_l|^p \leq 9^p \sum_{l \in I_\rho} |s_l|^p. \tag{2.23}$$

We sum over all triangles ρ in Δ. A certain s_l can appear more than once on the right–hand side and the number of times it appears can be bounded by the maximum number of triangles in the support of ϕ_l. We find

$$\|s(x,y)\|_p^p = \sum_{\rho \in \Delta} \int_\rho |s(x,y)|^p \leq \frac{2\pi}{\theta_\Delta}\, 9 \|\mathbf{s}\|_p^p, \tag{2.24}$$

which proves the upper bound in (2.20).

To prove the lower bound, we use the fact that all norms on a finite dimensional vector space are equivalent. Consider a triangle $\rho \in \Delta$ and the standard simplex $\rho_s := \{(x,y) : 0 \leq x, y \leq 1, x+y \leq 1\}$. We know that $\|s(x,y)\|_{\infty,\rho_s} \leq K_3 \|s(x,y)\|_{p,\rho_s}$ and therefor $\|s(x,y)\|_{\infty,\rho} \leq \frac{K_3}{A_\rho^{1/p}} \|s(x,y)\|_{p,\rho}$. Applying Theorem 2.1 gives

$$\begin{aligned} \sum_{l \in I_\rho} |s_l|^p &\leq \max_{l \in I_\rho} A_l \sum_{l \in I_\rho} |s_l A_l^{-1/p}|^p = \max_{l \in I_\rho} A_l \sum_{l \in I_\rho} |c_{ij}|^p \leq \max_{l \in I_\rho} A_l \; 9 \|\mathbf{c}\|_{\infty,\rho}^p \\ &\leq \max_{l \in I_\rho} A_l \; 9 K_1^p \|s(x,y)\|_{\infty,\rho}^p \leq \max_{l \in I_\rho} \frac{A_l}{A_\rho} \; 9 K_1^p K_3^p \|s(x,y)\|_{p,\rho}^p. \end{aligned} \tag{2.25}$$

Lemma 2.3 implies

$$\max_{l \in I_\rho} \frac{A_l}{A_\rho} \leq \frac{2\pi}{\theta_\Delta} K_2. \tag{2.26}$$

Summing over all triangles ρ in Δ yields

$$\|\mathbf{s}\|_p^p \leq \sum_{\rho \in \Delta} \sum_{l \in I_\rho} |s_l|^p \leq \frac{18\pi}{\theta_\Delta} K_1^p K_2 K_3^p \|s(x,y)\|_p^p, \tag{2.27}$$

which proves the lower bound in (2.20). □

3 Subdivision

In [17], Vanraes *et al.* present a subdivision scheme to compute a representation (2.19) of a Powell–Sabin spline on a refinement Δ^{j+1} of a triangulation Δ^j. The superscript j denotes the resolution level. The result is a denser set of control points $\mathbf{s}^{j+1}$. The corresponding new basis functions $\mathbf{\Phi}^{j+1}$ have smaller support than the basis functions $\mathbf{\Phi}^j$ on the previous level and each of the functions in $\mathbf{\Phi}^j$ can be written as a linear combination of the functions in $\mathbf{\Phi}^{j+1}$. We obtain a multiresolution analysis, an increasing sequence of subspaces can be associated with the base triangulation.

3.1 Triadic subdivision

Two new vertices are inserted on every edge and one new vertex is added inside each triangle, such that every edge is split in three and every triangle is split into nine new triangles. Remark that for the resulting refinement to exist, the interior point has to lie inside the hexagon formed by the six new vertices on the edges. It is always possible to place these new vertices such that this is fulfilled: there are no conditions on the initial triangulation Δ^j or its PS–refinement Δ_{PS}^j. The placement of the new vertices is illustrated in figure 2 for one triangle.

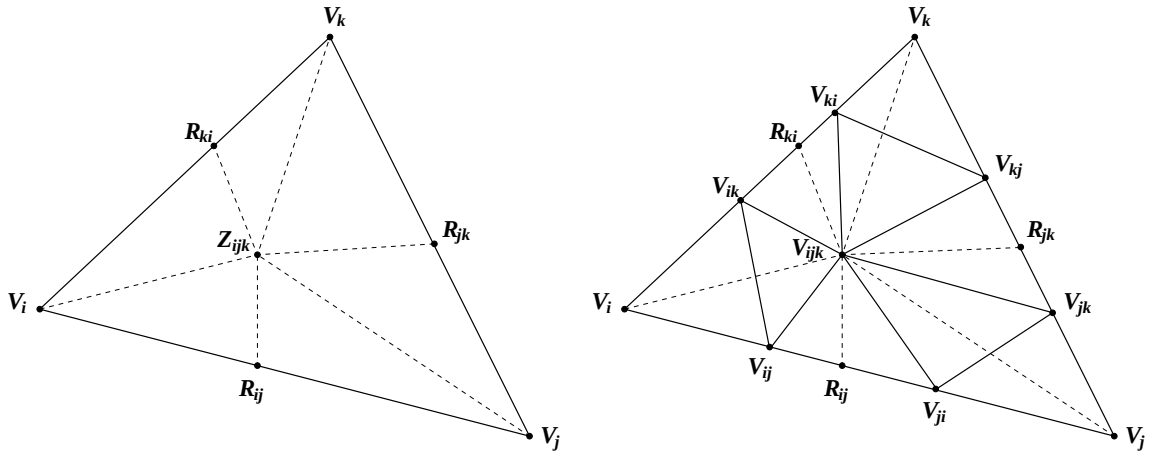


Figure 2. Principle of triadic subdivision. We place a new vertex at the position of the interior point and two new vertices on the edges each at one side of the intersection with the PS–refinement.

In [17] formulas are given to calculate the refined control points. The result can be written in block matrix form as

$$\mathbf{c}^{j+1} = \begin{bmatrix} \tilde{\mathbf{O}}^j \\ \tilde{\mathbf{N}}^j \end{bmatrix} \mathbf{c}^j. \tag{3.1}$$

We distinguish a part $\tilde{\mathbf{O}}^j$ that computes new control points for the old vertices that are contained in both Δ^j and Δ^{j+1}, and a part $\tilde{\mathbf{N}}^j$ that computes control points for the new vertices added when going from Δ^j to Δ^{j+1}. At this point it is important to remark that $\tilde{\mathbf{O}}^j$ is invertible, the new control triangle for an old vertex is in fact only a rescaled version of the old control triangle. Furthermore the subdivision formula are convex combinations, or in other words the rows of $\tilde{\mathbf{O}}^j$ and $\tilde{\mathbf{N}}^j$ contain a finite number of elements smaller than one and each row sums up to one. This means the subdivision algorithm is stable.

In terms of the normalised scaling coefficients (3.1) becomes

$$\mathbf{s}^{j+1} = \mathbf{P}^j \mathbf{s}^j \tag{3.2}$$

with

$$\mathbf{P}^j = \begin{bmatrix} \mathbf{O}^j \\ \mathbf{N}^j \end{bmatrix} = \mathbf{D}^{j+1} \begin{bmatrix} \tilde{\mathbf{O}}^j \\ \tilde{\mathbf{N}}^j \end{bmatrix} (\mathbf{D}^j)^{-1} = \begin{bmatrix} \mathbf{D}_o^{j+1} \tilde{\mathbf{O}}^j (\mathbf{D}^j)^{-1} \\ \mathbf{D}_n^{j+1} \tilde{\mathbf{N}}^j (\mathbf{D}^j)^{-1} \end{bmatrix}. \tag{3.3}$$

The matrix $\mathbf{P}^j$ is called the subdivision matrix and the diagonal matrices $\mathbf{D}^{j+1}$ and $\mathbf{D}^j$ are as defined in equation (2.18).

We also split $\mathbf{\Phi}^{j+1}$ in functions $\mathcal{O}^{j+1}$ associated with the old vertices in Δ^j and functions $\mathcal{N}^{j+1}$ associated with the new vertices added when going from Δ^j to Δ^{j+1}

$$\mathbf{\Phi}^{j+1} = [\mathcal{O}^{j+1} \mathcal{N}^{j+1}]. \tag{3.4}$$

3.2 Multiresolution analysis

The spline $s(x, y)$ can also be expanded in the refined basis

$$\begin{aligned} s(x,y) &= \mathbf{\Phi}^j \, \mathbf{s}^j \\ &= \mathbf{\Phi}^{j+1} \, \mathbf{s}^{j+1}. \end{aligned} \tag{3.5}$$

Combining (3.2) and (3.5) gives the relation between the basis functions on different levels

$$\mathbf{\Phi}^j = \mathbf{\Phi}^{j+1} \mathbf{P}^j. \tag{3.6}$$

This equation establishes refinebility since it states that each of the functions in $\mathbf{\Phi}^j$ can be written as a linear combination of the functions in $\mathbf{\Phi}^{j+1}$. Given this relation, a strictly increasing sequence of subspaces $V^j = S(\Delta^j_{PS})$ is associated with the base triangulation Δ^0

$$V^0 \subset V^1 \subset V^2 \ldots \tag{3.7}$$

This is called a multiresolution analysis (MRA).

The polynomial order of a MRA is the largest number $\tilde{N}$ for which $\Pi_{\tilde{N}-1}$, the space of bivariate polynomials of degree at most $\tilde{N} - 1$ on Ω, in contained in V^j

$$\tilde{N} = \max \{n \mid \Pi_{n-1} \subset V^j\}. \tag{3.8}$$

In the case of nested spaces of Powell–Sabin splines obviously $\tilde{N} = 3$.

A sequence of Riesz bases $\mathbf{\Phi}^j$ is uniformly stable if the Riesz bounds of $\mathbf{\Phi}^j$ are bounded away from 0 and from ∞ uniformly in j. We already know that the Riesz bounds depend only on the smallest angle θ_{Δ^j} in the triangulation Δ^j. From the construction of the refined triangulation Δ^{j+1} we know that the smallest angle cannot become arbitrary small and is at least $\theta > 0$ independent of j. The consecutive refinements are called shape regular.

4 Multiscale decomposition

In this section we discuss a filter bank algorithm to decompose a spline in V^{j+1} into a low resolution part in the coarser space V^j and a high resolution part that lives in a complement space W^j. The analysis and synthesis filters can easily be factored in lifting steps. The subdivision algorithm for the new vertices appears as one such lifting step. When doing this wavelet tranform the condition numbers should remain uniformly bounded.

4.1 Complement space

Each space V^{j+1} contains splines on a finer triangulation than the previous coarser space V^j and therefor can describe more detail of a surface. These details are captured in an algebraic complement W^j such that

$$V^j \oplus W^j = V^{j+1}, \tag{4.1}$$

where $\oplus$ denotes the inner sum of disjoint spaces. The complement space W^j is not necessarily orthogonal to V^j and we will refer to the basis functions $\mathbf{\Psi}^j$ of W^j as wavelets. In analogy with (3.6), the relation between $\mathbf{\Psi}^j$ and $\mathbf{\Phi}^{j+1}$ is given by a filter $\mathbf{Q}^j$

$$\mathbf{\Psi}^j = \mathbf{\Phi}^{j+1} \mathbf{Q}^j. \tag{4.2}$$

The wavelets are said to have N vanishing moments if W^j is orthogonal to Π_{N-1} for $j \geq j_0$.

4.2 Filter bank algorithm

Given a spline in V^{j+1}, we can decompose it into a low resolution part in V^j and a detail part in W^j as follows

$$\begin{aligned} s(x,y) &= \mathbf{\Phi}^{j+1}\mathbf{s}^{j+1} \\ &= \mathbf{\Phi}^{j}\mathbf{s}^{j} + \mathbf{\Psi}^{j}\mathbf{w}^{j}. \end{aligned} \tag{4.3}$$

This is done with two analysis filters, a low pass filter $\mathbf{A}^j$ and a high pass filter $\mathbf{B}^j$

$$\begin{aligned} \mathbf{s}^j &= \mathbf{A}^j\mathbf{s}^{j+1} \\ \mathbf{w}^j &= \mathbf{B}^j\mathbf{s}^{j+1}. \end{aligned} \tag{4.4}$$

Because

$$[\mathbf{\Phi}^j\ \mathbf{\Psi}^j] = \mathbf{\Phi}^{j+1}\,[\mathbf{P}^j\ \mathbf{Q}^j] \tag{4.5}$$

we can easily see that the analysis filters must be defined by the inverse relation

$$\begin{bmatrix}\mathbf{A}^j \\ \mathbf{B}^j\end{bmatrix}^{-1} = \begin{bmatrix}\mathbf{P}^j & \mathbf{Q}^j\end{bmatrix} \tag{4.6}$$

and $\mathbf{s}^{j+1}$ can be recovered from $\mathbf{s}^j$ and $\mathbf{w}^j$ using the synthesis filters $\mathbf{P}^j$ and $\mathbf{Q}^j$

$$\mathbf{s}^{j+1} = \mathbf{P}^j\mathbf{s}^j + \mathbf{Q}^j\mathbf{w}^j. \tag{4.7}$$

The filter operations are represented schematically in figure 4.2. The same procedure can now be repeated on the low pass coefficients $\mathbf{s}^j$ to yield $\mathbf{s}^{j-1}$ and $\mathbf{w}^{j-1}$ and to decompose V^j again in V^{j-1} and W^{j-1} and so on until level 0. Denote $\mathbf{M}^j = [\mathbf{P}^j\,\mathbf{Q}^j]$, then the matrix $\mathbf{T}^n$ that stands for the inverse transform from the multiscale representation to the fine scale data on level n is

$$\mathbf{s}^n = \mathbf{T}^n\,[\mathbf{s}^0\,\mathbf{w}^0\,\ldots\,\mathbf{w}^{n-1}\,\mathbf{w}^n]^T, \tag{4.8}$$

$$\mathbf{T}^n = \begin{bmatrix}\mathbf{M}^n & \mathbf{0} \\ \mathbf{0} & \mathbf{I}\end{bmatrix}\begin{bmatrix}\mathbf{M}^{n-1} & \mathbf{0} \\ \mathbf{0} & \mathbf{I}\end{bmatrix}\cdots\begin{bmatrix}\mathbf{M}^{0} & \mathbf{0} \\ \mathbf{0} & \mathbf{I}\end{bmatrix}. \tag{4.9}$$

In these equations $\mathbf{0}$ stands for the zero matrix, and $\mathbf{I}$ for the identity matrix.

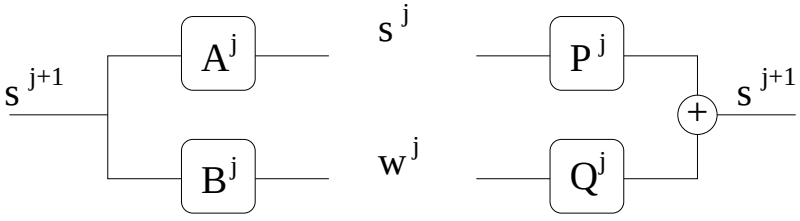


Figure 3. Filter bank algorithm.

4.3 Wavelet functions

The sets $\mathbf{\Phi^j}$ and $\mathcal{N}^{j+1}$ together span V^{j+1} because the matrix $\mathbf{O}^j$ is invertible. Obviously $\mathcal{N}^{j+1}$ can be used as wavelet functions

$$\mathbf{\Psi}^j = \mathcal{N}^{j+1} \quad \text{and} \quad \mathbf{Q}^j = \begin{bmatrix}\mathbf{0} \\ \mathbf{I}\end{bmatrix}. \tag{4.10}$$

By choosing the wavelet functions as the scaling functions on the finer level, we also made a choice for the complement space W^j. It can be desirable to have another complement space with certain properties as discussed in section 5. The wavelet functions can be found by projecting the $\mathcal{N}^{j+1}$ into the desired complement space W^j along V^j

$$\mathbf{\Psi}^j = \mathcal{N}^{j+1} - \mathbf{\Phi}^j \boldsymbol{\alpha}^j. \tag{4.11}$$

This projection is not necessarily orthogonal. For each wavelet function there is a corresponding column in $\boldsymbol{\alpha}^j$. The possibly nonzero entries in this column together will be called the stencil for that wavelet function. Remark that if there are no zero entries in $\boldsymbol{\alpha}^j$, the wavelets will have the whole domain Ω as their support.

4.4 Lifting

The reconstruction or synthesis filter in matrix form is now

$$\begin{bmatrix} \mathbf{P}^j & \mathbf{Q}^j \end{bmatrix} = \begin{bmatrix} \mathbf{O}^j & -\mathbf{O}^j\boldsymbol{\alpha}^j \\ \mathbf{N}^j & \mathbf{I} - \mathbf{N}^j\boldsymbol{\alpha}^j \end{bmatrix}. \tag{4.12}$$

Because $\mathbf{O}^j$ is invertible, the filterbank operation is also easily invertible and we find the analysis filters $\mathbf{A}^j$ and $\mathbf{B}^j$

$$\begin{bmatrix} \mathbf{A}^j \\ \mathbf{B}^j \end{bmatrix} = \begin{bmatrix} (\mathbf{O}^j)^{-1} - \boldsymbol{\alpha}^j\mathbf{N}^j(\mathbf{O}^j)^{-1} & \boldsymbol{\alpha}^j \\ -\mathbf{N}^j(\mathbf{O}^j)^{-1} & \mathbf{I} \end{bmatrix}. \tag{4.13}$$

These filters can be factored as follows

$$\begin{bmatrix} \mathbf{P}^j & \mathbf{Q}^j \end{bmatrix} = \begin{bmatrix} \mathbf{O}^j & \mathbf{0} \\ \mathbf{0} & \mathbf{I} \end{bmatrix} \cdot \begin{bmatrix} \mathbf{I} & \mathbf{0} \\ \mathbf{N}^j & \mathbf{I} \end{bmatrix} \cdot \begin{bmatrix} \mathbf{I} & -\boldsymbol{\alpha}^j \\ \mathbf{0} & \mathbf{I} \end{bmatrix} \tag{4.14}$$

and

$$\begin{bmatrix} \mathbf{A}^j \\ \mathbf{B}^j \end{bmatrix} = \begin{bmatrix} \mathbf{I} & \boldsymbol{\alpha}^j \\ \mathbf{0} & \mathbf{I} \end{bmatrix} \cdot \begin{bmatrix} \mathbf{I} & \mathbf{0} \\ -\mathbf{N}^j & \mathbf{I} \end{bmatrix} \cdot \begin{bmatrix} (\mathbf{O}^j)^{-1} & \mathbf{0} \\ \mathbf{0} & \mathbf{I} \end{bmatrix}. \tag{4.15}$$

This relates to the concept of lifting [14]. Every factor in the factorization of the filters corresponds to a lifting step. The filter bank factored in lifting steps is shown in figure 4.

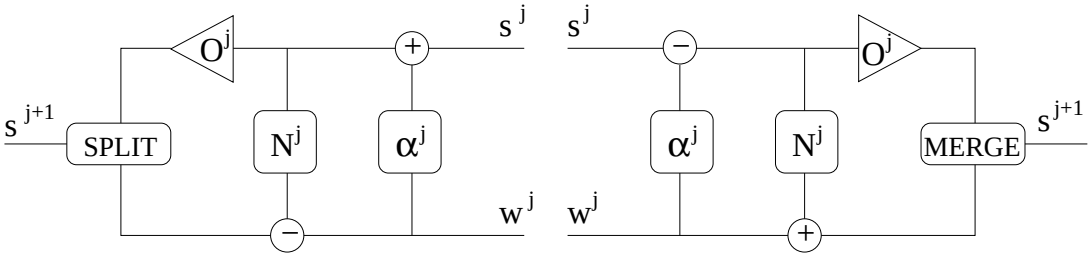


Figure 4. Filter bank factored in lifting steps.

First the control points $\mathbf{s}^{j+1}$ are split into two sequences. The first sequence, $\mathbf{s}_o^{j+1}$, contains the control points that correspond to vertices in Δ^j, and the second sequence, $\mathbf{s}_n^{j+1}$, contains control points that correspond to vertices that are in Δ^{j+1} but not in Δ^j. The subscripts o and n refer to old and new vertices during the subdivision process.

Then we want to treat $\mathbf{s}_o^{j+1}$ as the control points of a surface defined on Δ^j. Therefor we first need to scale the control triangles of the old vertices with $\mathbf{O}^{j^{-1}}$. After this we can apply the part $\mathbf{N}^j$ of the subdivision algorithm $\mathbf{P}^j$ that leads to the control points for the new vertices. The result is used as a prediction for $\mathbf{s}_n^{j+1}$ and substracted from this sequence. This yields the wavelet coefficients $\mathbf{w}^j$ on the lower branch in the picture. We call this step the prediction step. Finally $\mathbf{s}_o^{j+1}$ is updated with a linear combination defined by $\boldsymbol{\alpha}^j$ of wavelet coefficients $\mathbf{s}^j$. This yields the scaling coefficients $\mathbf{s}^j$ on the upper branch in the picture. We call this step the update step.

Reversing the lifting scheme is straightforward: we run through the scheme backwards, replace plus with minus signs, undo scaling operations and merge what had been split. So unlike the classical wavelet transform where $\mathbf{A}^j$, $\mathbf{B}^j$, $\mathbf{P}^j$ and $\mathbf{Q}^j$ are used explicitly, the same filters $\mathbf{O}^j$, $\mathbf{N}^j$ and $\boldsymbol{\alpha}^j$ appear now in the forward and inverse transform.

Note that we never compute the filters $\mathbf{O}^j$ and $\mathbf{N}^j$ explicitly nor do the matrix multiplication. Instead we apply the subdivision rules from [17] for each new vertex. As will become clear later also for the filter $\boldsymbol{\alpha}^j$ there is no matrix multiplication involved. The matrix $\boldsymbol{\alpha}^j$ will be calculated column by column and the old coefficients are updated incrementally.

4.5 Stability

When doing the wavelet transform there should be no significant loss of accuracy in the data, or in other words the condition numbers should remain uniformly bounded

$$\|\mathbf{T}^n\|, \|(\mathbf{T}^n)^{-1}\| = \mathcal{O}(1), \quad n \to \infty. \tag{4.16}$$

For an orthogonal wavelet transform this is automatically fulfilled. However, it suffices to have a orthogonal multiresolution decomposition in the sense that all complement spaces W^j are orthogonal complements of V^j in V^{j+1} and therefor also orthogonal to W^i with $i < j$. The basis functions need only be orthogonal between different levels and not within one level. We use in that case the term semiorthogonal wavelets in contrast with orthogonal wavelets.

From Dahmen [2] we know that the wavelet transform $\mathbf{T}^n$ is uniformly stable, i.e. (4.16) holds, if the multiscale basis $\bigcup_{j=1}^{\infty} \boldsymbol{\Psi}^j$ is also a Riesz basis for $\mathbf{L}_2$. A necessary condition is that each basis $\boldsymbol{\Psi}^j$ is a uniformly stable Riesz basis or alternatively that the condition numbers of the one level transforms $\mathbf{M}^j$ are uniformly bounded in j

$$\|\mathbf{M}^j\|, \|(\mathbf{M}^j)^{-1}\| = \mathcal{O}(1). \tag{4.17}$$

W^j is then called a stable complement of V^j in V^{j+1}. Remark that complement stability is not sufficient for the stability of the overall transform, because, in principle, the condition of the multiscale basis $\bigcup_{j=1}^{\infty} \Psi^j$ (4.16) may still become prohibitively large.

Dahmen establishes criteria for stability that are not based on Fourier techniques, so that they are useful for irregular and bounded domains. Certain Jackson and Bernstein inequalities must be satisfied from which we can see that the wavelets must have at least one vanishing moment. The DC-component must be conserved in the low pass signal. This is in accordance with results on the Sobolev regularity of refinable functions [1, 10]. The Sobolev exponent turns out to be strictly positive and proportional to the approximation order.

From these considerations we conclude that it is important to have at least one vanishing moment for the wavelets and that it is interesting to have a complement space W^j that is orthogonal to V^j.

5 Design of the update step

Without an update step the wavelet functions are the scaling functions on the next finer level corresponding to the new vertices. We use the update step to achieve the above mentioned properties that this unlifted wavelet functions do not have. We first overview some common choices for the update step. Then we describe our concrete approach and finally we define the inner product and explain how to compute it efficiently.

5.1 Update

A simple update from [14] is to obtain lifted wavelets with N vanishing moments, where N depends on the size of the stencil. The lifting coefficients $\boldsymbol{\alpha}^j$ are found as the solution of the $N \times N$-system that arises from the condition that the wavelet functions are orthogonal to a basis for Π_{N-1}. Unfortunately the magnitude of the lifting coefficients can be very sensitive to the choice of the stencil. The update coefficients in $\boldsymbol{\alpha}^j$ appear to be unbounded, and therefor the transform is not stable. Simoens gives examples of this phenomenon in the one dimensional case [12].

Another possibility would be to choose the update operator $\boldsymbol{\alpha}^j$ as the orthogonal projection from W^j into V^j. We then have a semiorthogonal multiresolution decomposition and (4.16) is satisfied. Because $\Pi_2 \subset V^j$ we immediately have two vanishing moments for free in this case. Unfortunately, to achieve semiorthogonality the width of the stencil cannot be limited, every scaling function in $\boldsymbol{\Phi}^j$ is involved in the update step. The resulting wavelet functions are not locally supported but stretch out over the whole domain Ω.

A third possibility is to fix the stencil and the scaling functions that come in the update step in advance and then orthogonalise each wavelet function to the subset of V^j that is defined by the stencil. Choosing the stencil is then a trade off between semiorthogonality and local support. A disadvantage of this idea is that we loose the two vanishing moments we had for free in the semiorthogonal case and we require at least one vanishing moment for stability.

5.2 Our approach

The solution we propose also fixes the stencil in advance in order to have local support for the wavelet functions. The stencil is different for a new vertex on the edge or a new vertex in the interior of an old triangle. Both stencils are shown in figure 5. A wavelet function of a new vertex on an edge is updated by the scaling functions of the two neighbouring old vertices on that edge. Because there are three basis functions associated with each vertex, the width of this stencil is six. For the wavelet function of a new vertex in the interior of an old triangle the scaling functions of the corners of the triangle are used. This yields a stencil of width nine.

We want to orthogonalise the wavelets to their predefined set of scaling functions, but we also want at least one vanishing moment. This leads to an overdetermined system because we do not have sufficient degrees of freedom

$$\mathbf{A} \cdot \boldsymbol{\alpha} = \mathbf{b} \quad \text{with} \quad \begin{cases} A_{k,l} &= \langle \phi_k^j, \phi_l^j \rangle \\ b_k &= \langle \phi_k^j, \mathcal{N}^{j+1} \rangle \end{cases} \tag{5.1}$$

$$\sum_{m=1}^{9} \langle 1, \phi_m^j \rangle \alpha_m = \langle 1, \mathcal{N}^{j+1} \rangle. \tag{5.2}$$

We could solve this system with an approximating method, but then the vanishing moment condition is not exactly fulfilled. Therefor we first solve equation (5.2) for α_1 and substitute α_1 in the remaining

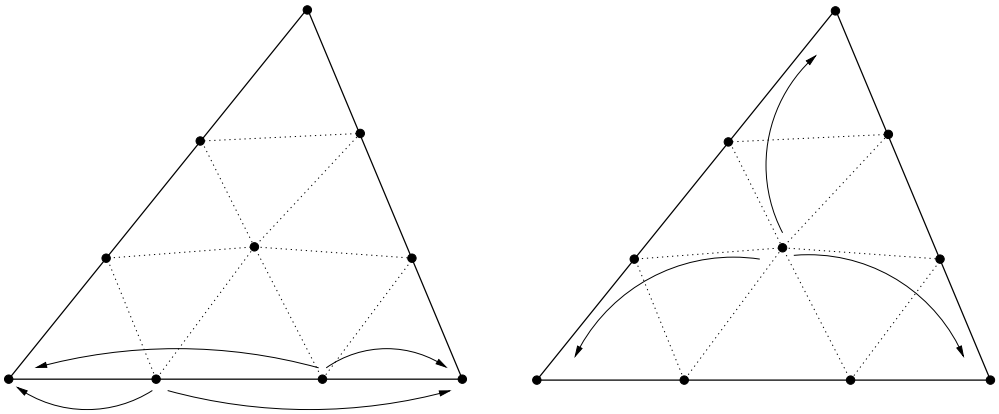


Figure 5. The update stencil is chosen a priori.

equations (5.1). The resulting system equals

$$\mathbf{A}' \cdot \boldsymbol{\alpha}' = \mathbf{b}' \quad \text{with} \quad \left\{ \begin{array}{rcl} A'_{k,l} & = & \langle \phi^j_k, \phi^j_{l+1} \rangle - \frac{\langle \phi^j_k, \phi^j_1 \rangle \langle 1, \phi^j_{l+1} \rangle}{\langle 1, \phi^j_1 \rangle} \\ \alpha'_l & = & \alpha_{l+1} \\ b'_k & = & \langle \phi^j_k, \mathcal{N}^{j+1} \rangle - \frac{\langle \phi^j_k, \phi^j_1 \rangle \langle 1, \mathcal{N}^{j+1} \rangle}{\langle 1, \phi^j_1 \rangle}. \end{array} \right. \tag{5.3}$$

This overdetermined system is then solved for $\boldsymbol{\alpha}'$ with a least squares method. The resulting wavelet function ψ^j has one vanishing moment and is as orthogonal as possible to its stencil of scaling functions in V^j.

5.3 Inner product

The inner product of two Powell–Sabin splines $f, g \in V^j$ is defined as

$$< f, g > := \int_{(x,y)\in\Omega} f(x,y) g(x,y) dx dy, \tag{5.4}$$

or, equivalently,

$$< f, g > := \sum_{\mathcal{T}^j \in \Delta^j_{PS}} \int_{(x,y)\in\mathcal{T}^j} f(x,y) g(x,y) dx dy. \tag{5.5}$$

Remark that some authors use the following alternative definition for the inner product

$$< f, g > := \sum_{\mathcal{T}^j \in \Delta^j(\Omega)} \frac{1}{\text{Area}(\mathcal{T}^j)} \int_{(x,y)\in\mathcal{T}^j} f(x,y) g(x,y)\ dx dy. \tag{5.6}$$

The latter definition implies that triangles of different geometric size and shape are weighted equally. The resulting wavelet spaces are invariant of the geometry of the mesh and consequently a significant amount of precomputation of inner products is possible. However, in the case of Powell–Sabin subdivision the scaling functions depend on the PS–triangle which can be different for each vertex. Therefor no precompution is possible. Moreover, we prefer the first definition because it does not ignore the inherent irregularity of the triangulation.

The practical computation of the inner product is done by considering one triangle $\mathcal{T}^j \in \Delta^j_{PS}$ at the time. The functions $f|_{\mathcal{T}^j}$ and $g|_{\mathcal{T}^j}$ are bivariate polynomials of degree ≤ 2 and have a unique

Bézier representation

$$f|_{\mathcal{T}^j}(x,y) := b(\tau) = \sum_{|\lambda|=2} b_\lambda B^2_\lambda(\tau), \tag{5.7}$$

with $\lambda = (\lambda_1, \lambda_2, \lambda_3)$, $\lambda_i \geq 0$ a multi–index of length $|\lambda| = \lambda_1 + \lambda_2 + \lambda_3 = 2$ and $\tau = (\tau_1, \tau_2, \tau_3)$ the barycentric coordinates of a point $(x, y) \in \mathbb{R}^2$ with respect to $\mathcal{T}^j$. The functions $B^n_\lambda(\tau)$ are the Bernstein–Bézier polynomials and the coefficients b_λ are the Bézier ordinates associated with the domain points $(\frac{\lambda_1}{2}, \frac{\lambda_2}{2}, \frac{\lambda_3}{2})$.

This Bézier representation can be obtained easily from the B–spline representation [8]. Denote the Bézier ordinates of $f|_{\mathcal{T}^j}$ and $g|_{\mathcal{T}^j}$ as b_λ and c_λ respectively, then

$$\begin{aligned}\int_{(x,y)\in\mathcal{T}^j} f(x,y)g(x,y)dxdy &= \int_{\mathcal{T}^j} \sum_{|\lambda|=2} b_\lambda B^2_\lambda(\tau) \sum_{|\lambda|=2} \tilde{b}_\lambda B^2_\lambda(\tau)\ d\tau, \\ &= \int_0^1 \int_0^{1-\tau_1} |J(\tau)| \sum_{|\lambda|=2} b_\lambda B^2_\lambda(\tau) \sum_{|\lambda|=2} \tilde{b}_\lambda B^2_\lambda(\tau)\ d\tau_2 d\tau_1, \end{aligned} \tag{5.8}$$

where the Jacobian $|J(\tau)|$ equals $2 \cdot \text{Area}(\mathcal{T}^j)$. Some elementary calculus yields

$$\int_{(x,y)\in\mathcal{T}^j} f(x,y)g(x,y)dxdy = \text{Area}(\mathcal{T}^j) \begin{bmatrix} c_{200} \\ c_{110} \\ c_{020} \\ c_{011} \\ c_{002} \\ c_{101} \end{bmatrix}^T \begin{bmatrix} \frac{1}{15} & \frac{1}{30} & \frac{1}{90} & \frac{1}{90} & \frac{1}{90} & \frac{1}{30} \\ \frac{1}{30} & \frac{2}{45} & \frac{1}{30} & \frac{1}{45} & \frac{1}{90} & \frac{1}{45} \\ \frac{1}{90} & \frac{1}{30} & \frac{1}{15} & \frac{1}{30} & \frac{1}{90} & \frac{1}{90} \\ \frac{1}{90} & \frac{1}{45} & \frac{1}{30} & \frac{2}{45} & \frac{1}{30} & \frac{1}{45} \\ \frac{1}{90} & \frac{1}{90} & \frac{1}{90} & \frac{1}{30} & \frac{1}{15} & \frac{1}{30} \\ \frac{1}{30} & \frac{1}{45} & \frac{1}{90} & \frac{1}{45} & \frac{1}{30} & \frac{2}{45} \end{bmatrix} \begin{bmatrix} b_{200} \\ b_{110} \\ b_{020} \\ b_{011} \\ b_{002} \\ b_{101} \end{bmatrix}. \tag{5.9}$$

Substituting (5.9) in (5.5) yields the inner product.

6 Results

6.1 Wavelets

Figure 6 shows a wavelet function corresponding to a new vertex in the interior of an old triangle. On the left we see the wavelet before the update step, it is the corresponding scaling function on the finer level. On the right we see the wavelet after the update step. The wavelet now has a vanishing moment, the integral equals zero. Remark that with every vertex there are three scaling functions or wavelet functions, each for one corner of the control triangle. This explains the larger lob in the front. The sum of the three basis functions is balanced.

6.2 Stability

Theorem 6.1 *The one level transforms* $\mathbf{M}^j$ *are uniformly bounded in* j

$$\|\mathbf{M}^j\|, \|(\mathbf{M}^j)^{-1}\| = \mathcal{O}(1), \tag{6.1}$$

with $\|\cdot\|$ *the* $\mathbf{L}_2$ *norm.*

Proof.

(1) From the factorisations (4.14) and (4.15) we know it is sufficient to prove

$$\|\boldsymbol{\alpha}^j\|, \|\mathbf{N}^j\|, \|\mathbf{O}^j\|, \|\mathbf{O}^{j^{-1}}\| = \mathcal{O}(1). \tag{6.2}$$



(a) (b)

Figure 6. (a) Wavelet function before update is scaling function on finer level. (b) Wavelet function after update.

Since an arbitrary matrix $\mathbf{F}$ satisfies the property $\|\mathbf{F}\|^2 \leq \|\mathbf{F}\|_1 \|\mathbf{F}\|_\infty$, we will look for upper bounds for $\|\cdot\|_1$ and $\|\cdot\|_\infty$.

(2) From the construction of the update step it follows that $\boldsymbol{\alpha}^j$ is a sparse matrix. Each column has maximal nine non–zero entries, and each row has maximal $3 \cdot \frac{2\pi}{\theta_{\Delta^j}}$ non–zero entries. It follows that $\|\boldsymbol{\alpha}^j\|_1 \leq 9 \max_{kl} |\alpha^j_{kl}|$ and $\|\boldsymbol{\alpha}^j\|_\infty \leq \frac{6\pi}{\theta_{\Delta^j}} \max_{kl} |\alpha^j_{kl}|$, or

$$\|\boldsymbol{\alpha}^j\| \leq 3\sqrt{\frac{6\pi}{\theta_{\Delta^j}}} \max_{kl} |\alpha^j_{kl}|. \tag{6.3}$$

(3) To derive an upper bound for $\max_{kl} |\alpha^j_{kl}|$ we define $\mathbf{A}$, $\boldsymbol{\alpha}$ and $\mathbf{b}$ as in section 5.4. The column vector $\boldsymbol{\alpha}$ that is part of the update matrix $\boldsymbol{\alpha}^j$ satisfies

$$\mathbf{A} \cdot \boldsymbol{\alpha} = \mathbf{b} + \boldsymbol{\epsilon} \quad \text{with } \boldsymbol{\epsilon} \text{ the least squares error,} \tag{6.4}$$

$$\sum_{m=1}^{9} < 1, \phi^j_m > \alpha_m =< 1, \mathcal{N}^{j+1} > . \tag{6.5}$$

Clearly $\mathbf{A}$ is a Gram matrix. Suppose that $\{\phi^{*j}_1, \ldots, \phi^{*j}_9\}$ is a dual base for $\{\phi^j_1, \ldots, \phi^j_9\}$, i.e. $< \phi^j_k, \phi^{*j}_l >= \delta_{kl}$, and suppose that $\phi^{*j}_l =: \sum_{k=1}^9 b_{kl} \phi^j_k$, then $\mathbf{A}^{-1} = (b_{kl})$ and

$$\|\phi^{*j}_l\|^2 =< \phi^{*j}_l, \phi^{*j}_l >=< \phi^{*j}_l, \sum_{k=1}^{9} b_{kl} \phi^j_k >= b_{ll}. \tag{6.6}$$

From the $\mathbf{L}_2$ stability of $\boldsymbol{\Phi}^j$ it follows that $k_1^2 \sum_{k=1}^9 b^2_{kl} \leq \|\phi^{*j}_l\|^2$, with k_1 a constant only depending on θ_{Δ^j}. So $k_1^2 \sum_{k=1}^9 b^2_{kl} \leq b_{ll}$ and we derive

$$|b_{kl}| \leq \frac{1}{k_1^2}. \tag{6.7}$$

Because of (6.4)

$$\|\boldsymbol{\alpha}\|_\infty \leq \|\mathbf{A}^{-1}\|_\infty (\|\mathbf{b}\|_\infty + \|\boldsymbol{\epsilon}\|_\infty). \tag{6.8}$$

Combining (6.6), (6.7) and (6.8) gives

$$\max_i |\alpha_i| \leq \frac{9}{k_1^2}(1 + \|\boldsymbol{\epsilon}\|_\infty). \tag{6.9}$$

(4) Suppose that

$$\forall i: \ \alpha_i = \frac{< 1, \mathcal{N}^{j+1} >}{\sum_{m=1}^{9} < 1, \phi_m^j >}, \tag{6.10}$$

then $\alpha_i = \mathcal{O}(1)$ and $\|\boldsymbol{\epsilon}\| = \|\mathbf{A} \cdot \boldsymbol{\alpha} - \mathbf{b}\| = \mathcal{O}(1)$. Since the least squares method finds an $\boldsymbol{\alpha}$ that minimizes $\|\mathbf{A} \cdot \boldsymbol{\alpha} - \mathbf{b}\|$, we have a contradiction if we suppose that $\|\boldsymbol{\epsilon}\|_\infty \neq \mathcal{O}(1)$. Hence $\|\boldsymbol{\epsilon}\|_\infty = \mathcal{O}(1)$ and

$$\max_{kl} |\alpha_{kl}^j| \leq \frac{9k_3}{k_1^2}, \tag{6.11}$$

with k_3 a constant.

(5) According to (3.3), $\mathbf{N}^j$ can be written as $\mathbf{D}_n^{j+1}\tilde{\mathbf{N}}^j(\mathbf{D}^j)^{-1}$, with $\tilde{\mathbf{N}}^j$ a sparse matrix. Because the subdivision scheme only uses convex combinations, we know that all entries in $\tilde{\mathbf{N}}^j$ are smaller than one. Every row in $\mathbf{N}^j$ corresponds to a function in $\mathcal{N}^{j+1}$ and every column to a function in $\boldsymbol{\Phi}^j$. The $(k,l) - th$ entry of $\mathbf{N}^j$ is non–zero if and only if the support of $\mathcal{N}_k^{j+1}$ lies in the support of ϕ_l^j. Suppose that the (k,l)th entry is non–zero, then it is bounded by $\sqrt{A_{\mathcal{N}_k^{j+1}}/A_{\phi_l^j}}$ which is $\mathcal{O}(1)$. Hence $\|\mathbf{N}^j\| = \mathcal{O}(1)$.

(6) We recall from (3.3) that $\mathbf{O}^j$ can be written as $\mathbf{D}_o^{j+1}\tilde{\mathbf{O}}^j(\mathbf{D}^j)^{-1}$. To prove the boundedness of $\|\mathbf{O}^j\|$ similar arguments can be used as in (5). We also need $\|(\mathbf{O}^j)^{-1}\| = \mathcal{O}(1)$. Again we find that it is sufficient to prove that $\sqrt{A_{\phi_l^j}/A_{\phi_l^{j+1}}} = \mathcal{O}(1)$. This follows easily from Lemma 2.3.

6.3 Condition numbers

Table 1 gives condition numbers for an example with six triangles on level 0 in the 1–norm and table 2 for the ∞–norm. The condition numbers for the scaling and the prediction are upper bounds, the condition numbers for the update are exact.

$\|\cdot\|_1$	level j				
	0	1	2	3	4
$\kappa\left(\begin{bmatrix} \mathbf{O}^j & \mathbf{0} \\ \mathbf{0} & \mathbf{I} \end{bmatrix}\right)$	43,821	43,666	43,702	43,714	43,714
$\kappa\left(\begin{bmatrix} \mathbf{I} & \mathbf{0} \\ \mathbf{N}^j & \mathbf{I} \end{bmatrix}\right)$	11,419	13,018	13,019	13,019	13,019
$\kappa\left(\begin{bmatrix} \mathbf{I} & -\alpha^j \\ \mathbf{0} & \mathbf{I} \end{bmatrix}\right)$	20,305	17,128	17,128	17,128	17,128

Table 1. Condition numbers in 1-norm

7 Conclusion

In this paper we presented a new wavelet transform for Powell–Sabin splines based on the lifting scheme. The proposed scheme consists of two lifting steps. The first step uses an existing subdivision algorithm to predict the in between values, such that quadratic polynomial functions are exactly reproduced. The second step updates the old values to achieve one vanishing moment and to make the wavelets as orthogonal as possible to their predefined stencil of scaling functions.

$\|\cdot\|_\infty$	level j				
	1	2	3	4	5
$\kappa\left(\begin{bmatrix} \mathbf{O}^j & \mathbf{0} \\ \mathbf{0} & \mathbf{I} \end{bmatrix}\right)$	2,4981	2,4935	2,4936	2,4936	2,4936
$\kappa\left(\begin{bmatrix} \mathbf{I} & \mathbf{0} \\ \mathbf{N}^j & \mathbf{I} \end{bmatrix}\right)$	11,431	15,021	15,022	15,022	15,022
$\kappa\left(\begin{bmatrix} \mathbf{I} & -\alpha^j \\ \mathbf{0} & \mathbf{I} \end{bmatrix}\right)$	212,31	262,49	262,50	262,50	262,51

Table 2. Condition numbers in ∞-norm

The wavelets are locally supported because the width of the stencil in the update step is limited. We used a weighted inner product that takes into account the actual geometric size of the triangles which is better for the least squares accuracy. Throughout the construction we paid attention to stability issues. The scaling functions are normalised with respect to their support to form a Riesz basis for the 2–norm. We also give a proof of the stability of the wavelet transform.

A wavelet decomposition algorithm based on subdivision can only be used for splines on triangulations with subdivision connectivity. This is also referred to as semiregular meshes. These meshes can be the output of a remeshing algorithm or other applications based on subdivision.

Acknowledgement

This work is partially supported by the Belgian Program on Interuniversity Poles of Attraction, initiated by the Belgian State, Prime Minister's Office for Science, Technology and Culture, and by the Flemish Fund for Scientific Research (FWO VLaanderen) project MISS (G.0211.02). The scientific responsibility rests with the authors.

Bibliography

1. A. Cohen, K. Grochenig, and L.F. Villemoes. Regularity of multivariate refinable functions. *Constructive Approximation*, 15:241–255, 1999.
2. W. Dahmen. Some remarks on multiscale transformations, stability and orthogonality. In P.J. Laurent, A. L. Méhauté, and L.L. Schumaker, editors, *Curves and Surfaces II*, pages 1–32. A.K. Peters, Boston, 1991.
3. I. Daubechies and W. Sweldens. Factoring wavelet transforms into lifting steps. *J. Fourier Anal. Appl.*, 4(3):245–267, 1998.
4. P. Dierckx. On calculating normalized Powell–Sabin B–splines. *CAGD*, 15(3):61–78, 1997.
5. G. Farin. Triangular Bernstein–Bézier patches. *CAGD*, 3(2):83–128, 1986.
6. Michael Lounsbery, Tony D. DeRose, and Joe Warren. Multiresolution analysis for surfaces of arbitrary topological type. *ACM Transactions on Graphics*, 16(1):34–73, 1997.
7. J. Maes, E. Vanraes, P. Dierckx, and A. Bultheel. On the stability of normalized Powell-Sabin B-splines. *J. Comput. Appl. Math.*, Submitted, 2003.
8. P.Dierckx, S. Van Leemput, and T. vermeire. Algorithms for surface fitting using Powell-Sabin splines. *IMA J. Numer. Anal.*, 12:271–299, 1992.
9. M. J. D. Powell and M. A. Sabin. Piecewise quadratic approximations on triangles. *ACM Transactions on Mathematical Software*, 3:316–325, 1977.

10. A. Ron and Z. Shen. The sobolev regularity of refinable functions. *J. Approx. Theory*, 106(2):185–225, 1997.
11. X. Shi, S. Wang, W. Wang, and R. H. Wang. The C^1 quadratic spline space on triangulations. *Report 86004, Department of Mathematics, Jilin University, Changchun*, 1986.
12. Jo Simoens and Stefan Vandewalle. A stabilized lifting construction of wavelets on irregular meshes on the interval. *SIAM J. Sci. Comput.*, To Appear.
13. W. Sweldens. The lifting scheme: A custom-design construction of biorthogonal wavelets. *Appl. Comput. Harmon. Anal.*, 3(2):186–200, 1996.
14. W. Sweldens. The lifting scheme: A construction of second generation wavelets. *SIAM J. Math. Anal.*, 29(2), 1997.
15. E. Vanraes, P. Dierckx, and A. Bultheel. On the choice of the PS–triangles. TW Report 353, Department of Computer Science, Katholieke Universiteit Leuven, Belgium, 2003.
16. E. Vanraes, M. Jansen, and A. Bultheel. Stabilized wavelet transforms for nonequispaced data smoothing. *Signal Processing*, 82(12):1979–1990, 2002.
17. E. Vanraes, J. Windmolders, A. Bultheel, and P. Dierckx. Subdivision for Powell–Sabin spline surfaces. TW Report 345, Department of Computer Science, Katholieke Universiteit Leuven, Belgium, September 2002.
18. J. Windmolders, E. Vanraes, P. Dierckx, and A. Bultheel. Uniform Powell-Sabin spline wavelets. *Journal Computational Applied Mathematics*, 154(1):125–142, 2003. Accepted.